The Astrophysical Journal Letters, 799:L23 (6pp), 2015 January 30 doi:10.1088/2041-8205/799/2/L23

THE MASS-DEPENDENCE OF ANGULAR MOMENTUM EVOLUTION IN SUN-LIKE STARS

Sean P. Matt[1], A. Sacha Brun[2], Isabelle Baraffe[1,3], Jérôme Bouvier[4,5], and Gilles Chabrier[1,3]

[1] Department of Physics and Astronomy, University of Exeter, Physics Building, Stocker Road, Exeter, EX4 4QL, UK; s.matt@exeter.ac.uk

[2] Laboratoire AIM Paris-Saclay, CEA/Irfu Université Paris-Diderot CNRS/INSU, F-91191 Gif-sur-Yvette, France

[3] École Normale Supérieure de Lyon, CRAL, F-69364 Lyon Cedex 07, France

[4] Université de Grenoble Alpes, IPAG, F-38000 Grenoble, France

[5] CNRS, IPAG, F-38000 Grenoble, France

Received 2014 September 21; accepted 2014 December 12; published 2015 January 29

ABSTRACT

To better understand the observed distributions of the rotation rate and magnetic activity of Sun-like and low-mass stars, we derive a physically motivated scaling for the dependence of the stellar wind torque on the Rossby number. The torque also contains an empirically derived scaling with stellar mass (and radius), which provides new insight into the mass-dependence of stellar magnetic and wind properties. We demonstrate that this new formulation explains why the lowest mass stars are observed to maintain rapid rotation for much longer than solar-mass stars, and simultaneously why older populations exhibit a sequence of slowly rotating stars, in which the low-mass stars rotate more slowly than solar-mass stars. The model also reproduces some previously unexplained features in the period–mass diagram for the *Kepler* field, notably: the particular shape of the "upper envelope" of the distribution, suggesting that ∼95% of *Kepler* field stars with measured rotation periods are younger than ∼4 Gyr; and the shape of the "lower envelope," corresponding to the location where stars transition between magnetically saturated and unsaturated regimes.

Key words: magnetohydrodynamics (MHD) – stars: evolution – stars: late-type – stars: magnetic field – stars: rotation – stars: winds, outflows

1. INTRODUCTION

This Letter presents a formulation for the global angular momentum loss of Sun-like stars, defined here as stars with less than $\sim 1.3\ M_\odot$, which have outer convective envelopes and are magnetically active. The goal is to develop a comprehensive physical model for the evolution of stellar angular momentum that (1) explains both the age-dependence and mass-dependence of observed stellar spin rate distributions and (2) is fully consistent with our current best understanding of stellar wind dynamics, magnetic properties, and mass-loss rates.

The work is both motivated and enabled by large samples of stellar rotation periods, now existing for several clusters, spanning an age range of $\sim 10^{6-9}$ yr (Irwin & Bouvier 2009; Bouvier et al. 2014). When plotted in period–color (or period–mass) diagrams, the distributions exhibit a complex but apparently coherent evolution with cluster age (Barnes 2003). This evolution includes a relatively smooth dependence on stellar mass, from $\sim 1.3\ M_\odot$ down to the substellar limit. In general, during the first several hundred megayears, lower mass stars take longer to spin down than higher mass stars. Second, and somewhat paradoxically, after ∼100 Myr, the slowest rotators begin to converge toward a narrow "sequence" in which the lower mass stars rotate more slowly than higher mass stars. This behavior, particularly of the slowly rotating sequence, gave birth to gyrochronology (Barnes 2003; Soderblom 1983; Skumanich 1972), the idea that stellar ages may be inferred solely from rotation period and mass. Gyrochronology will become increasingly important for recent and future data sets (e.g., from exoplanet transit searches) that provide rotation period measurements of large samples of stars with unknown ages. The best current example is the measurement of 34,000 rotation periods in the *Kepler* mission field of view by Mcquillan et al. (2014).

The present model builds upon many previous works, including theoretical developments of how magnetized stellar winds remove angular momentum (Schatzman 1962; Mestel 1968; Weber & Davis 1967; Kawaler 1988; Matt et al. 2012), models for the evolution of stellar spin rate in time (e.g., MacGregor & Brenner 1991; Denissenkov et al. 2010; Scholz et al. 2011; Reiners & Mohanty 2012; Gallet & Bouvier 2013; van Saders & Pinsonneault 2013; Brown 2014), and gyrochronology relations (Barnes 2003, 2010; Mamajek & Hillenbrand 2008; Meibom et al. 2009).

Much of the difficulty in predicting stellar wind torques arises from the uncertainty (both observational and theoretical) in our knowledge of the magnetic and stellar wind properties of stars. Despite significant progress in measurements of the mass-loss rates of Sun-like stars (Wood et al. 2005), theoretical predictions of wind properties (Suzuki et al. 2013; Cranmer & Saar 2011), mapping of the surface magnetic fields (Donati & Landstreet 2009), and dynamo models (Miesch & Toomre 2009; Brun et al. 2014), we are still working to understand how these properties depend upon stellar mass, rotation rate, and time. Observations of various indicators of magnetic activity (Noyes et al. 1984a; Reiners et al. 2009; Pizzolato et al. 2003; Mamajek & Hillenbrand 2008; Wright et al. 2011; Vidotto et al. 2014), as well as theoretical models for magnetic field generation (Durney & Latour 1978; Noyes et al. 1984b; Baliunas et al. 1996; Jouve et al. 2010), suggest that a key parameter for stellar magnetism is the Rossby number,

$$Ro \equiv (\Omega_* \tau_{cz})^{-1}, \quad (1)$$

where Ω_* is the angular rotation rate of the star, and τ_{cz} is the convective turnover timescale, characterized by the size of a convective region divided by the convective velocity. For slowly rotating stars, magnetic properties appear to correlate strongly with Ro. Below a critical value of the Rossby number, $Ro_{\rm sat}$, various magnetic activity indicators appear to "saturate" in the sense that they have an approximately constant maximal value (independent of Ro). The value at which the saturated/

unsaturated transition occurs can be specified by a constant

$$\chi \equiv \frac{Ro_\odot}{Ro_{\rm sat}} \equiv \frac{\Omega_{\rm sat}\tau_{cz}}{\Omega_\odot \tau_{cz\odot}}, \quad (2)$$

where "$\odot$" refers to solar values. Saturation occurs for $Ro \leqslant Ro_\odot/\chi$, and χ defines the critical rotation rate, $\Omega_{\rm sat}$ (or period $P_{\rm sat} \equiv 2\pi/\Omega_{\rm sat}$), for any star with known $\tau_{cz}/\tau_{cz\odot}$. The various studies cited above suggest that χ lies in the approximate range of 10–15.

The model presented here reproduces some previously unexplained features in period–mass diagrams and also places constraints on the scaling of magnetic activity with Rossby number and stellar mass.

2. STELLAR WIND TORQUE MODEL

2.1. General Formulation

Models of stellar wind dynamics (Kawaler 1988; Matt et al. 2012) show that the torque on the star can be written generically,

$$T = T_\odot \left(\frac{M_*}{M_\odot}\right)^{-m} \left(\frac{R_*}{R_\odot}\right)^{5m+2} \times \left(\frac{B_*}{B_\odot}\right)^{4m} \left(\frac{\dot{M}_w}{\dot{M}_\odot}\right)^{1-2m} \left(\frac{\Omega_*}{\Omega_\odot}\right), \quad (3)$$

where M_* and R_* are the stellar mass and radius, B_* the magnetic field strength on the stellar surface, and $\dot{M}_w$ the global mass outflow rate. The exponent factor m is determined primarily by the magnetic field geometry and wind acceleration profile (Réville et al. 2015) and likely falls in the range $m = 0.20$–0.25 (Washimi & Shibata 1993; Matt & Pudritz 2008; Ud-Doula et al. 2009; Pinto et al. 2011; Matt et al. 2012).

Given the uncertainties in both B_* and $\dot{M}_w$, we adopt a generic combined relationship based upon the rotation activity phenomenology discussed in Section 1,

$$\left(\frac{B_*}{B_\odot}\right)^{4m} \left(\frac{\dot{M}_w}{\dot{M}_\odot}\right)^{1-2m} = Q \left(\frac{Ro_\odot}{Ro}\right)^{p} \quad \text{(unsaturated)}, \quad (4)$$

$$\left(\frac{B_*}{B_\odot}\right)^{4m} \left(\frac{\dot{M}_w}{\dot{M}_\odot}\right)^{1-2m} = Q\chi^{p} \quad \text{(saturated)}, \quad (5)$$

which inherits the degeneracy between B_* and $\dot{M}_w$ from Equation (3). The exponent p encapsulates the dependence of this combined activity factor on the Rossby number. The generic scale factor Q has a yet unknown dependence on stellar parameters, which is determined empirically in Section 2.2.

A combination of Equations (1)–(5) results in a bifurcated equation for the stellar wind torque,

$$T = -T_0 \left(\frac{\tau_{cz}}{\tau_{cz\odot}}\right)^{p} \left(\frac{\Omega_*}{\Omega_\odot}\right)^{p+1} \quad \text{(unsaturated)}, \quad (6)$$

$$T = -T_0 \chi^{p} \left(\frac{\Omega_*}{\Omega_\odot}\right) \quad \text{(saturated)}, \quad (7)$$

where $T_0 = T_0(T_\odot, M_*, R_*, Q, m)$ does not depend upon the spin rate or τ_{cz}. For the remainder of this work, we adopt $\chi = 10$, consistent with rotation activity relationships and within the range used in spin-evolution models cited in Section 1. We also adopt $p = 2$, which gives the unsaturated spin scaling ($T \propto \Omega_*^3$) most commonly used in the literature. Table 1 lists the values of all adopted parameters in the present work.

Table 1
Adopted Parameter Values

Symbol	Adopted Value	Description
χ	10	Inverse critical Rossby number for magnetic saturation (solar units)
p	2	Rotation activity scaling, Equation (4)
$M_\odot$	1.99×10^{33} g	Solar mass
$R_\odot$	6.96×10^{10} cm	Solar radius
$\Omega_\odot$	2.6×10^{-6} Hz	Solar (solid body) angular rot. rate
$I_\odot$	1.05×10^{54} g cm^2	Solar moment of inertia
$t_\odot$	4.55×10^{9} yr	Solar age
$\tau_{cz\odot}$	12.9 days	Normalization for conv. turnover time

2.2. Observationally Inferred Torque Scaling

It is clear from the derivation above that T_0 should have a complex dependence on stellar parameters, depending on m and Q. Given the uncertainty associated with these quantities, we used the observed stellar spin rates to infer a dependence of T_0 on stellar mass. We tested various scalings for T_0 and settled on one that is a compromise between physical motivation and simplicity. Specifically, we adopt

$$T_0 = 9.5 \times 10^{30} \text{ erg } \left(\frac{R_*}{R_\odot}\right)^{3.1} \left(\frac{M_*}{M_\odot}\right)^{0.5}. \quad (8)$$

For the empirically derived scaling of Equation (8) to be consistent with Equations (3)–(7), the general formulation requires that $T_\odot = 9.5 \times 10^{30}$ erg and

$$Q = \left(\frac{R_*}{R_\odot}\right)^{3.1-(5m+2)} \left(\frac{M_*}{M_\odot}\right)^{0.5+m}. \quad (9)$$

2.3. Analysis of Spin Down in Time

Using the torque defined by Equations (6)–(8), we can now solve an angular momentum equation to obtain the spin rate of any star as a function of time, t. Under the simplifying assumptions of solid body rotation and that the stellar moment of inertia, I_*, is constant in time (approximately true for main-sequence stars), there are analytic solutions given by

$$\Omega_* = \Omega_i e^{-t/\tau_{\rm sat}} \quad \text{(saturated)}, \quad (10)$$

$$\lim_{\Omega_* \ll \Omega_{\rm sat}} \left(\frac{\Omega_*}{\Omega_\odot}\right) \rightarrow \left(\frac{\tau_{\rm unsat}}{t}\right)^{\frac{1}{p}} \quad \text{(unsaturated)}, \quad (11)$$

where Ω_i is the "initial" spin rate corresponding in practice to some very young age ($t \ll \tau_{\rm sat}$), and two spin-down timescales are defined as

$$\tau_{\rm sat} \equiv \frac{I_*\Omega_\odot}{T_0 \chi^{p}} \quad (12)$$

$$\tau_{\rm unsat} \equiv \frac{I_*\Omega_\odot}{T_0 p} \left(\frac{\tau_{cz\odot}}{\tau_{cz}}\right)^{p}. \quad (13)$$

Equation (11) predicts the spin rate only in the asymptotic limit of $\Omega_* \ll \Omega_{\rm sat}$. Stars generally begin their lives with rotation rates in the saturated regime. Equation (10) then applies until a time when the spin rate decreases to the critical spin rate, $\Omega_{\rm sat}$, after which all spin rates asymptotically converge and approach Equation (11). This converged spin rate is independent of the initial value, Ω_i, and decreases as a simple power law in time, reproducing the Skumanich (1972) relationship for $p = 2$.

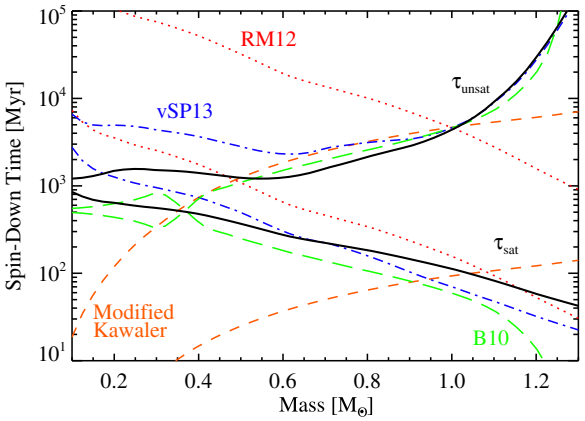

Figure 1. Spin-down time in the saturated (lower solid line; fast-rotation) and unsaturated (upper solid line; slow-rotation) regimes vs. stellar mass. The overall slope of τ vs. M_* has an opposite sign in each regime. This slope change explains why lower mass stars remain rapid rotators for longer than higher mass stars and, simultaneously, why slowly rotating stars form a sequence in which the lower mass stars rotate more slowly than higher mass stars. The broken lines show the two spin-down times for other models in the literature: dashed—modified Kawaler formulation (e.g., van Saders & Pinsonneault 2013); long-dashed—Barnes (2010, B10); dotted—Reiners & Mohanty (2012, RM12); dot-dashed—van Saders & Pinsonneault (2013, vSP13).

To illustrate the effect of the torque in each regime, Figure 1 shows the spin-down times (Equations (12) and (13)), as a function of stellar mass. For the figure, we use values of I_* from stellar models of Baraffe et al. (1998) at an age of 2 Gyr, and compute τ_{cz} using the model effective temperatures with Equation (36) of Cranmer & Saar (2011). The saturated spin-down time (lower line) represents the *e*-folding time of the spin rate, since the spin down is approximately exponential (Equation (10)). Once stars are in the unsaturated regime, τ_{unsat} (upper line) corresponds to the age at which the converged spin rate equals the solar rate, $\Omega_\odot$; τ_{unsat} also predicts the mass-dependence of the converged spin rates at any age (according to Equation (11)).

Since χ and p are constants, the difference in the mass-dependence of τ_{sat} and τ_{unsat} is due *entirely* to the factor of τ_{cz}^p (appearing only in τ_{unsat}). This difference is enough to reverse the sense of the mass-dependence in the two regimes: higher mass stars spin down the most quickly in the saturated regime, but in the unsaturated regime, lower mass stars spin down the most quickly.

Figure 1 also shows the equivalent spin-down times for some models in the literature, with τ_{unsat} normalized to the Sun. Of these, the vSP13 and B10 models are the most similar to the present model in both saturated and unsaturated regimes. However, all models differ by more than a factor of two in some mass range. All models therefore predict significantly different spin down behavior, and the present model has been tuned (via Equation (8)) to best reproduce the observed phenomenology presented in Section 3. The key strength of the present model is its formulation, which connects the observed spin evolution to the scaling of magnetic field strengths and mass-loss rates.

3. EVOLUTION OF A SYNTHETIC CLUSTER

3.1. Initial Conditions

To compare with observations, we computed the evolution of stellar spin rates for a synthetic cluster of 500 stars. We started the evolution from an age of 5 Myr in order to avoid the earliest phases, where the spin distributions are poorly understood (and likely due to processes not included here). The cluster initially has a random and uniform distribution in stellar mass (in the range 0.1–1.3 $M_\odot$) and in the logarithm of rotation period (in the range 0.8–15 days). The left panel of Figure 2 shows this initial distribution, compared with the ∼2 Myr old cluster ONC (data from Stassun et al. 1999; Herbst et al. 2001, 2002; Rodríguez-Ledesma et al. 2009). The figure demonstrates that the initial conditions approximate the general range of rotation periods observed in young clusters, with no attempt to fit or explain the detailed distribution.

3.2. Spin Evolution

Starting from the initial condition, we solved the angular momentum equation

$$\frac{d\Omega_*}{dt} = \frac{T}{I_*} - \frac{\Omega_*}{I_*}\frac{dI_*}{dt}, \quad (14)$$

for each star, using a forward-timestepping Euler method, and assuming solid-body rotation. The torque was specified by Equations (6)–(8) (and Equation (2) determining the saturated/unsaturated transition) and values in Table 1. At each timestep, we interpolated the stellar parameters R_*, I_*, and dI_*/dt from a grid of pre-computed (non-rotating) stellar evolution tracks of Baraffe et al. (1998) and computed τ_{cz} from the prescription of Cranmer & Saar (2011).

The evolution proceeds as follows. During the first several tens of megayears, all stars are contracting and spin up by a factor of 5–10, as they approximately conserve angular momentum (the torques are negligible on this timescale). When the stars reach the main sequence, their structure stabilizes and they begin their spin down. Once $\Omega_* < \Omega_{sat}$, their spin rates rapidly converge toward the asymptotic spin rate predicted by Equation (11). This evolution and the formation of a converged, slow-rotator sequence occurs first for the highest mass stars and proceeds in a continuous manner toward lower masses. Figure 2 (right panel) and Figure 3 show the synthetic cluster after it has evolved to ages between 500 Myr and 4 Gyr.

3.3. Comparison with Observations

3.3.1. Praesepe Cluster

The right panel of Figure 2 compares the rotation periods in the ∼580 Myr old Praesepe cluster (observed by Agüeros et al. 2011) to the synthetic cluster at a similar age. Two key observed features are reproduced by the synthetic cluster. First, there is a population of rapid rotators, exhibiting a wide range of rotation rates and a trend such that the lowest mass stars are, on average, more rapidly rotating than higher mass stars. In the models, the wide range is a consequence of the initial distribution, but the trend with mass is due to the fact that lower mass stars take longer to spin down in the saturated regime (see Figure 1).

The second feature reproduced by the models is the population of stars that have converged onto a relatively narrow sequence (following an approximate upper limit in period). In the models, the existence of a converged sequence is due to the stars entering the unsaturated regime, where the torque depends strongly upon rotation rate. The trend of rotation rate with mass is due to the fact that lower mass stars generally spin down quicker than higher mass stars once in the unsaturated regime (Figure 1).

A few observed features are not reproduced by the model. The first is a handful of stars rotating more rapidly than the

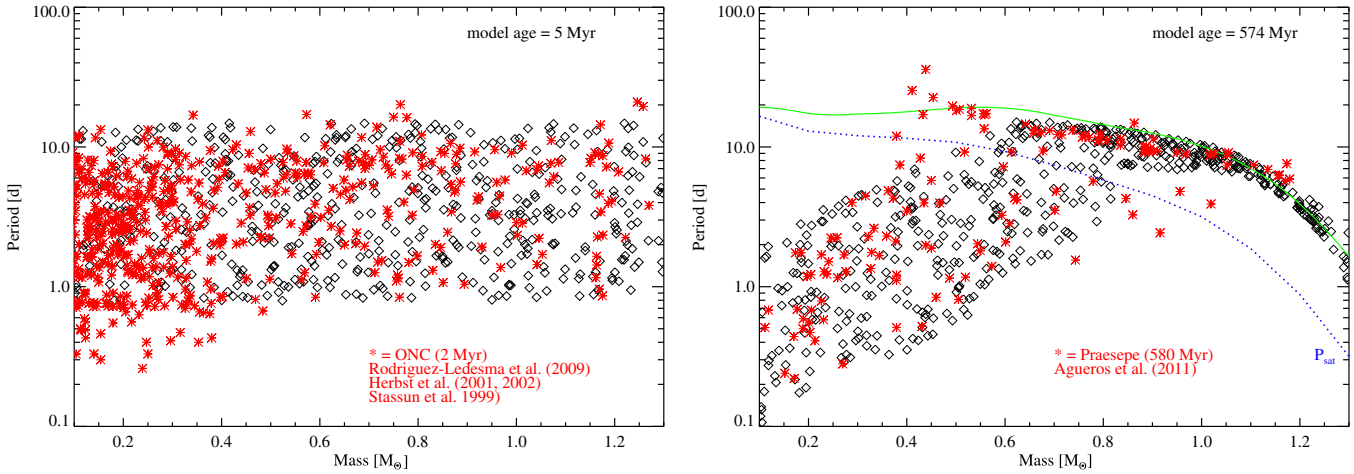

Figure 2. Observed rotation periods (red stars) from the ONC (left panel) and Praesepe (right panel) compared to our synthetic cluster stars (black diamonds). The left panel shows the synthetic initial conditions, chosen to approximate the observed range, but not the detailed distribution. The right panel shows the synthetic cluster, evolved to a similar age as Praesepe (as indicated). For reference, the green solid line shows the theoretical asymptotic spin rate of Equation (11), and the blue dotted line delimits magnetically saturated and unsaturated stars. The model explains both the existence of rapidly rotating, low-mass stars, as well as the general mass-dependence of the slow-rotator sequence.

synthetic cluster stars (in the range 0.7–1 $M_\odot$), which suggests a modified torque for these stars. Second is the population of slow rotators (in the range 0.35–0.6 $M_\odot$) that appear to extend the slow-rotator sequence to lower masses than in the synthetic cluster. This discrepancy likely arises from a deviation from solid-body rotation (which the model assumes). Studies that included internal angular momentum transport (MacGregor & Brenner 1991; Gallet & Bouvier 2013; Charbonnel et al. 2013; Denissenkov 2010) indicate that internal differential rotation manifests as an increased spin down at early times, followed by a convergence toward the solid-body solution at later times. The predicted asymptotic spin rate (green line in Figure 2) roughly traces the observed sequence over its full mass range, giving support for the mass-dependence of the torque, even though the solid-body approximation does not capture all details.

3.3.2. *Kepler* Field

Figure 3 compares the measured rotation periods in the *Kepler* field (Mcquillan et al. 2014, hereafter MMA14) to the synthetic cluster, shown at three different ages. The figure only shows stars with measured rotation periods, comprising 26% of the total *Kepler* main-sequence sample, and possessing a range of unknown ages. Within the framework of our model, we interpret some broad features of the observed spin distribution in the *Kepler* field.

First, there is a well-defined "upper envelope" to the distribution of observed rotation periods (corresponding approximately to the 95th percentile of the distribution), which coincides with the 4 Gyr old synthetic cluster, for stars with $\gtrsim$0.5 $M_\odot$, including the apparent "dip" or change in slope around 0.6 $M_\odot$. This dip has not been previously reproduced by any model. The coincidence with the model suggests that the existence and shape of the observed upper envelope is real (rather than being due to observational bias) and also corresponds to an age of ~4 Gyr (also noted by MMA14). At masses below 0.5 $M_\odot$, the mismatch between the synthetic cluster and observations indicates that the low-mass, unsaturated stars require a stronger torque than the model predicts.

There is also a relatively sharp "lower envelope" in the observed distribution of Figure 3, also noted by MMA14, most pronounced for stars with $\lesssim$0.9 $M_\odot$. This lower envelope has not been previously explained, but it corresponds remarkably well to the location of the critical rotation period (blue dotted line), which delineates the saturated and unsaturated regimes in our model. As is apparent in the right panel of Figure 2, the spin rates of stars begin to converge after crossing this critical rotation period. Thus, in a distribution of stars with a range of ages, the model predicts that the density of stars will increase at a rotation period slightly larger than the critical period, as observed. Recall that the critical rotation period (Equation (2)) is set by a constant saturation level, χ, and the mass-dependent convective turnover timescale, τ_{cz}. Thus, the coincidence of $P_{\rm sat}$ with the lower envelope of the *Kepler* spin distribution supports the modeled relationship between convection, magnetic activity (including saturation), and spin evolution. Furthermore, *independent of any model*, the lower envelope coincides precisely with the slow-rotator sequence observed in the youngest clusters in which this feature appears (those with ages of ~100 Myr, not shown; Bouvier et al. 2014). This comparison with young clusters, as well as with the present model, suggests that the *Kepler* field has a substantial population of stars with ages less than ~500 Myr (also noted by MMA14).

4. DISCUSSION AND CONCLUSIONS

The model presented here builds upon the ideas and successes of many previous works (cited in Section 1), notably in the explanation for a saturation of the torque at high spin rates and a Skumanich-style spin down at later times. However, the present model provides a new formulation that reproduces some previously unexplained phenomena, particularly related to the mass-dependence of observed features in Figures 2 and 3.

A number of observed phenomena that are not reproduced by the model will require further improvements; for example, the model does not well produce the *Kepler* field slow rotators for masses below 0.5 $M_\odot$, which suggests (for example) that the adopted values of τ_{cz} may not be appropriate for these stars; the overall interpretation of the *Kepler* field star ages (Section 3.3.2) should be tested by population studies; a fraction of stars (e.g., in Praesepe) appear to converge onto the unsaturated sequence at an earlier time than the models, suggesting a deviation from

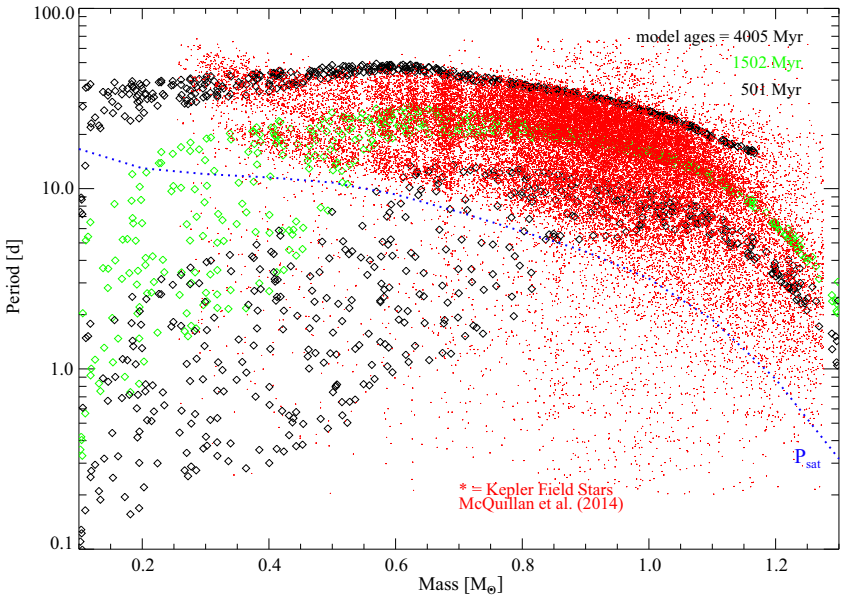

Figure 3. Observed rotation periods in the *Kepler* field (red symbols), plotted over the syntetic cluster, shown at three different ages: 500 Myr (lower group of black diamonds), 1.5 Gyr (green diamonds), and 4.0 Gyr (upper group of black diamonds). The blue dotted line shows the rotation period dividing the saturated and unsaturated regimes. The coincidence of $P_{\rm sat}$ with the "lower envelope" of the *Kepler* stars, suggests that this feature is explained by the convergence of stellar spin rates, occurring after stars enter the unsaturated regime. The coincidence of the oldest models with the observed "upper envelope" suggests that ∼95% of the sample stars are younger than ∼4 Gyr.

solid-body rotation; and the present model does not explain the "initial" conditions or any of the more detailed structure present in the spin distributions of young stars (see Herbst et al. 2001; Henderson & Stassun 2012; Brown 2014).

Much of the success of the present model derives from the empirical mass-scaling of the torque, given by Equation (8). This is not a unique solution, and the physics suggest a dependence on more complex stellar properties than M_* and R_* (e.g., $\dot{M}_w$ may depend on coronal Alfvén wave flux; Cranmer & Saar 2011). However, for any other formulation to work as well, the included physics must conspire to scale like Equation (8).

Fitting the present model to observations provides constraints on the physical parameters $\dot{M}_w$, B_*, χ, p, and m, all of which are connected to the physics and phenomenology of magnetic properties and wind dynamics in Sun-like stars. For the parameters adopted here and a dipolar magnetic field (i.e., $m = 0.22$), the model's torque could arise from the simple scalings[6] $B_* \propto Ro^{-1}$ and $\dot{M}_w \propto M_*^{1.3} Ro^{-2}$. These scalings can be compared to models and observations and do not appear unreasonable. Thus, a key advantage of our formulation is that it provides a basic framework for a self-consistent physical picture of stellar evolution that includes the effects of magnetic activity, mass loss, and rotation.

The EU's FP7 supported S.P.M. and A.S.B. under grant No. 207430 "STARS2" (http://www.stars2.eu), I.B. under grant #320478 "TOFU, and G.C. under grant #247060" J.B. and A.S.B. were supported by the grant ANR 2011 Blanc SIMI5-6 02001 "TOUPIES" (http://ipag.osug.fr/Anr_Toupies/).

REFERENCES

Agüeros, M. A., Covey, K. R., Lemonias, J. J., et al. 2011, ApJ, 740, 110
Baliunas, S. L., Nesme-Ribes, E., Sokoloff, D., & Soon, W. H. 1996, ApJ, 460, 848
Baraffe, I., Chabrier, G., Allard, F., & Hauschildt, P. H. 1998, A&A, 337, 403
Barnes, S. A. 2003, ApJ, 586, 464
Barnes, S. A. 2010, ApJ, 722, 222
Bouvier, J., Matt, S. P., Mohanty, S., et al. 2015, in Protostars and Planets VI (Tucson, AZ: Univ. Arizona Press), in press arXiv:1309.7851
Brown, T. M. 2014, ApJ, 789, 101
Brun, A. S., Garcia, R. A., Houdek, G., Nandy, D., & Pinsonneault, M. 2014, SSRv, November, 54
Charbonnel, C., Decressin, T., Amard, L., Palacios, A., & Talon, S. 2013, A&A, 554, 40
Cranmer, S. R., & Saar, S. H. 2011, ApJ, 741, 54
Denissenkov, P. A. 2010, ApJ, 719, 28
Denissenkov, P. A., Pinsonneault, M., Terndrup, D. M., & Newsham, G. 2010, ApJ, 716, 1269
Donati, J.-F., & Landstreet, J. D. 2009, ARA&A, 47, 333
Durney, B. R., & Latour, J. 1978, GApFD, 9, 241
Gallet, F., & Bouvier, J. 2013, A&A, 556, 36
Henderson, C. B., & Stassun, K. G. 2012, ApJ, 747, 51
Herbst, W., Bailer-Jones, C. A. L., & Mundt, R. 2001, ApJL, 554, L197
Herbst, W., Bailer-Jones, C. A. L., Mundt, R., Meisenheimer, K., & Wackermann, R. 2002, A&A, 396, 513
Irwin, J., & Bouvier, J. 2009, in IAU Symp. 258, The Ages of Stars, ed. E. E. Mamajek, D. R. Soderblom, & R. F. G. Wyse (Cambridge: Cambridge Univ. Press), 363
Jouve, L., Brown, B. P., & Brun, A. S. 2010, A&A, 509, A32
Kawaler, S. D. 1988, ApJ, 333, 236
MacGregor, K. B., & Brenner, M. 1991, ApJ, 376, 204
Mamajek, E. E., & Hillenbrand, L. A. 2008, ApJ, 687, 1264
Matt, S., & Pudritz, R. E. 2008, ApJ, 678, 1109
Matt, S. P., MacGregor, K. B., Pinsonneault, M. H., & Greene, T. P. 2012, ApJL, 754, L26
Mcquillan, A., Mazeh, T., & Aigrain, S. 2014, ApJS, 211, 24, (MMA14)
Meibom, S., Mathieu, R. D., & Stassun, K. G. 2009, ApJ, 695, 679
Mestel, L. 1968, MNRAS, 138, 359
Miesch, M. S., & Toomre, J. 2009, AnRFM, 41, 317
Noyes, R. W., Hartmann, L. W., Baliunas, S. L., Duncan, D. K., & Vaughan, A. H. 1984a, ApJ, 279, 763
Noyes, R. W., Weiss, N. O., & Vaughan, A. H. 1984b, ApJ, 287, 769
Pinto, R. F., Brun, A. S., Jouve, L., & Grappin, R. 2011, ApJ, 737, 72
Pizzolato, N., Maggio, A., Micela, G., Sciortino, S., & Ventura, P. 2003, A&A, 397, 147
Reiners, A., Basri, G., & Browning, M. 2009, ApJ, 692, 538
Reiners, A., & Mohanty, S. 2012, ApJ, 746, 43
Réville, V., Brun, A. S., Matt, S., Strugarek, A., & Pinto, R. 2015, ApJ, 798, 116

[6] Formally, Equations (4) and (9) define a family of solutions satisfying $B_*^{4m} \dot{M}_w^{1-2m} \propto R_*^{3.1-(5m+2)} M_*^{0.5+m} Ro^{-p}$. We give one possibility here.

Rodríguez-Ledesma, M. V., Mundt, R., & Eislöffel, J. 2009, A&A, 502, 883
Schatzman, E. 1962, AnAp, 25, 18
Scholz, A., Irwin, J., Bouvier, J., et al. 2011, MNRAS, 413, 2595
Skumanich, A. 1972, ApJ, 171, 565
Soderblom, D. R. 1983, ApJS, 53, 1
Stassun, K. G., Mathieu, R. D., Mazeh, T., & Vrba, F. J. 1999, AJ, 117, 2941
Suzuki, T. K., Imada, S., Kataoka, R., et al. 2013, PASJ, 65, 98
Ud-Doula, A., Owocki, S. P., & Townsend, R. H. D. 2009, MNRAS, 392, 1022
van Saders, J. L., & Pinsonneault, M. H. 2013, ApJ, 776, 67
Vidotto, A. A., Gregory, S. G., Jardine, M., et al. 2014, MNRAS, 441, 2361
Washimi, H., & Shibata, S. 1993, MNRAS, 262, 936
Weber, E. J., & Davis, L. 1967, ApJ, 148, 217
Wood, B. E., Müller, H.-R., Zank, G. P., Linsky, J. L., & Redfield, S. 2005, ApJL, 628, L143
Wright, N. J., Drake, J. J., Mamajek, E. E., & Henry, G. W. 2011, ApJ, 743, 48